

Dynamical energy analysis on mesh grids: a new tool for describing the vibro-acoustic response of complex mechanical structures

D.J. Chappell^{a,*}, D. Löchel^b, N. Søndergaard^b, G. Tanner^c

^a*School of Science and Technology, Nottingham Trent University, Nottingham NG11 8NS, UK*

^b*inuTech GmbH, Fürther Str. 212, 90429 Nürnberg, Germany*

^c*School of Mathematical Sciences, University of Nottingham, Nottingham NG7 2RD, UK*

Abstract

We present a new approach for modelling noise and vibration in complex mechanical structures in the mid-to-high frequency regime. It is based on a dynamical energy analysis (DEA) formulation which extends standard techniques such as statistical energy analysis (SEA) towards non-diffusive wave fields. DEA takes into account the full directionality of the wave field and makes sub-structuring obsolete. It can thus be implemented on mesh grids commonly used, for example, in the finite element method (FEM). The resulting mesh based formulation of DEA can be implemented very efficiently using *discrete flow mapping* (DFM) as detailed in [1] and described here for applications in vibro-acoustics. A mid-to-high frequency vibro-acoustic response can be obtained over the whole modelled structure. Abrupt changes of material parameter at interfaces are described in terms of reflection/transmission matrices obtained by solving the wave equation locally. Two benchmark model

*Corresponding author

Email address: david.chappell@ntu.ac.uk (D.J. Chappell)

systems are considered: a double-hull structure used in the ship-building industry and a cast aluminium shock tower from a Range Rover. We demonstrate that DEA with DFM implementation can handle multi-mode wave propagation effectively, taking into account mode conversion between shear, pressure and bending waves at interfaces, and on curved surfaces.

Keywords: Statistical Energy Analysis, Ray Tracing, Transfer operators

1. Introduction

A vast range of numerical methods have been developed for solving noise and vibration problems in mechanical structures. Popular tools include finite element methods, finite volume methods, boundary element methods and various spectral methods. There are, however, basic limitations when approximating the solutions of wave equations directly: the size of the associated linear system increases with decreasing wavelength and numerical schemes become inefficient when the local wavelengths are orders of magnitude smaller than typical dimensions of the physical system. One therefore moves to high frequency methods, such as ray tracing. However, tracking rays including multiple reflections on boundaries can become cumbersome, in particular on curved surfaces and when including mode conversion at interfaces.

These problems can partly be circumvented by using statistical approaches. Dividing the structure into a set of substructures and assuming diffuse wave fields and quasi-equilibrium conditions in each of the resulting subsystems leads to greatly simplified set of equations based only on coupling constants between subsystems. This idea forms the basis of statistical energy analysis

(SEA) [2], which has found widespread applications in the automotive and aviation industry, as well as in architectural acoustics. The disadvantage of SEA is that the underlying assumptions are often hard to verify a-priori, or are only justified when an additional averaging over equivalent subsystems is considered. These shortcomings have been addressed by Langley [3] and more recently by Le Bot [4, 5]. A computational tool based on a linear operator approach for propagating ray densities called dynamical energy analysis (DEA) has been proposed in [6]. DEA systematically interpolates between SEA and full ray tracing. The name points at the similarities with SEA but stresses at the same time the importance of non-diffusive transport along the ray dynamics. In particular, in DEA we have much more freedom in sub-structuring the total system and variations of the energy density across sub-structures can be resolved.

The implementation of DEA as presented in [6, 7] corresponds to a spectral boundary integral method; the integral equations are expanded using orthogonal basis approximations and the resulting matrix equations are solved for the coefficients of the basis expansion of the solution. In [8], it has been shown that using a boundary element method for the spatial variable and a basis function expansion in the momentum coordinate leads to efficiency gains. In DEA, coupling between subsystems is described in terms of reflection/transmission matrices. These matrices are obtained by solving the wave equation locally in the coupling region. The interfaces can be, for example, line junctions between plates of different thickness or junctions between plates and stiff components, where the local wavelength is of the same order as the size of the component.

We will demonstrate that the method can be implemented efficiently on a mesh with thousands of subelements including multi-mode wave propagation. Due to the geometric simplicity of typical (planar) mesh elements, DEA can be modified using the method of *Discrete Flow Mapping* (DFM) [1] which gives rise to huge efficiency gains. DEA provides then detailed resolution of the energy density variation throughout the structure under consideration. The method is applied to benchmark problems provided by Germanischer Lloyd (part of a double-hull structure of a large ship) [9] and Jaguar Land Rover (cast aluminium shock tower of a Range Rover). In these examples, mode mixing between in-plane and bending modes is incorporated.

2. Dynamical energy analysis – a brief overview

2.1. From ray tracing to flow equations - an operator formulation

We present a brief overview of the problem set-up and methodology, for more details see [6, 7, 8, 10]. We consider linear wave problems driven by a distribution of sources at a fixed angular frequency ω ; a generalisation to frequency band excitation is straightforward and is discussed below. The total system is defined on a domain Ω , which is divided into a set of sub-domains $\Omega_j, j = 1, \dots, N_\Omega$, such as the elements of a mesh grid. The material parameters and hence the local wave speeds are assumed to be constant in each sub-domain, but may vary between sub-domains. Damping is incorporated through a complex-valued damping term μ , which may depend on ω . In general, one needs to determine the solution u of a wave equation (where u is, for example, the displacement within a solid or pressure variations within

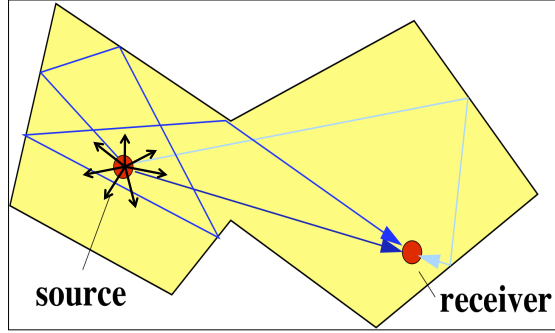


Figure 1: Ray tracing including reflection at boundaries

a fluid) of the form

$$\left(\hat{H} + \omega^2\right) u(r) = -f(r). \quad (1)$$

Here, \hat{H} corresponds to a linear operator describing the vibro-acoustic dynamics including dissipation, and f represents an excitation driving the system. Appropriate boundary conditions apply at the outer boundaries and at the interfaces between sub-domains. The wave energy density ϵ at a point r is then proportional to the square of the wave amplitude $|u|$, that is,

$$\epsilon(r, \omega) \propto |u(r, \omega)|^2. \quad (2)$$

The linear wave equation (1) can in a natural way be associated with the ray dynamics via the Eikonal approximation expressing the wave function u in terms of ray contributions [6, 8] with associated amplitude A_j and phase ψ_j , $j = 1, 2, \dots$. This leads to a double sum over ray trajectories for the wave

energy density of the form

$$\begin{aligned}
\epsilon(r, \omega) &\propto \sum_{j,j'} A_j(r, \omega) A_{j'}(r, \omega) \cos(\omega(\psi_j(r) - \psi_{j'}(r))) \\
&= \sum_j A_j(r, \omega)^2 + \sum_{j \neq j'} A_j(r, \omega) A_{j'}(r, \omega) \cos(\omega(\psi_j(r) - \psi_{j'}(r))).
\end{aligned} \tag{3}$$

Taking the average over a frequency band centered on ω_0 such that the second summation becomes negligibly small, then the mean wave energy density is well approximated by the density of rays $\rho(r, p, \omega_0)$ passing through a point r , hence

$$\begin{aligned}
\bar{\epsilon}(r, \omega_0) &\propto \sum_j \bar{A}_j(r, \omega_0)^2 \\
&= \int \rho(r, p; \omega_0) dp,
\end{aligned} \tag{4}$$

where p is the direction (or momentum) vector, the magnitude of which is related to the wavenumber. From hereon we consider problems with a fixed frequency excitation, where this frequency must be interpreted as the centre frequency ω_0 of a band average. The system is excited by one or more point sources from which rays emerge uniformly and undergo reflections at boundaries as well as absorption processes, see Fig. 1. It is therefore possible to relate wave energy densities to classical flow equations and thus thermodynamical concepts, which are at the heart of SEA and DEA treatments. Note that different mode types such as shear, pressure or bending modes in plates are treated as rays with different local wave speed. Mode coupling at boundaries or interfaces leads to mode-conversion of rays, that is, the classical flow of rays will undergo ray-splitting. The conversion rates between rays corresponding to different modes are related to the modulus square of the entries

of an interface scattering matrix. Likewise, the transmission/reflection probabilities between sub-domains are given by the ratios of the outgoing normal power fluxes to the incoming normal power flux at the interface, which can again be obtained from the scattering matrix.

DEA is based on the observation that these flow equations for ray densities can also be described using linear partial differential equations, namely the phase space Liouville equation (LE) [8]. In order to solve the stationary flow problem we rewrite the LE in boundary integral form; the boundary can be the physical boundary of the system and/or the union of interfaces between the sub-domains. Note that when implemented on a mesh grid, the total boundary consists of the union of all mesh element boundaries. For simplicity, let us first consider a single domain with boundary Γ . We map the ray density emanating continuously from the source points onto the boundary. The resulting boundary density is equivalent to a source density on the boundary producing the same ray field in the interior as the original source field after one reflection.

Ray densities ρ emanating from the boundary are transported to the next intersection with the boundary by the operator \mathcal{B} ,

$$\mathcal{B}[\rho](X_s) := w(X_s)\rho(\varphi^{-1}(X_s)) = \int w(Y_s)\delta(X_s - \varphi(Y_s))\rho(Y_s)dY_s. \quad (5)$$

Here $X_s = (s, p_s)$ (and Y_s) represent phase-space coordinates on the boundary, that is, s parameterises the boundary Γ and p_s denotes the direction (or momentum) component tangential to Γ at s . Also φ is the boundary map (see fig. 2); it takes a ray from a boundary point s with tangential direction component p_s along the straight line path to the next intersection with the boundary. Note that φ is invertible in convex (sub-) domains. The weight

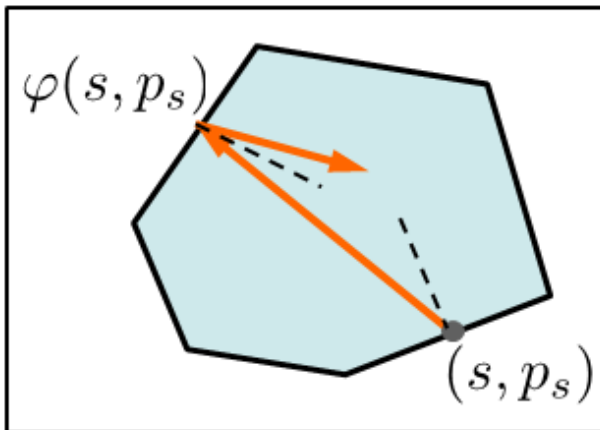


Figure 2: Transfer of ray densities by the boundary map φ

function $w(X_s)$ contains absorption factors as well as reflection/transmission coefficients. The stationary density on the boundary induced by an initial boundary distribution $\rho_\Gamma^0(X_s)$ is then obtained using

$$\rho_\Gamma = \sum_{n=0}^{\infty} \mathcal{B}^n[\rho_\Gamma^0] = (I - \mathcal{B})^{-1}[\rho_\Gamma^0], \quad (6)$$

where B^n contains trajectories undergoing n reflections at the boundary. The density distribution in the interior region can then be obtained from the boundary density ρ_Γ . One obtains the density (4) after projecting down onto coordinate space.

Note that the treatment sketched above is formally equivalent to ray tracing. A generalisation to multi-domain problems with sub-domains $\Omega_j, j = 1, \dots, N_\Omega$ is straightforward by introducing a multi-domain boundary map φ_{ij} and weight function w_{ij} describing the flow from the boundary of domain Ω_i to the boundary of Ω_j . The operator \mathcal{B} is then constructed from the set of inter-domain operators \mathcal{B}_{ij} .

2.2. A basis representation for the ray tracing operator \mathcal{B}

In the following we restrict our discussion to two-dimensional problems, an implementation for the three-dimensional case is described in [10]. In order to evaluate (6), a finite dimensional approximation of the operator \mathcal{B} is constructed. We approximate the boundary density using basis functions. For the spatial variable s , piecewise constant boundary element functions on the (discretised) boundary are used [8, 10]. For the approximation in the momentum argument we choose a Legendre polynomial basis. Note that in two dimensions, the variable $p_s \in (-|p|, |p|)$ in general with $|p|$ on the energy surface defined through $H(p, r) = \omega_0^2$, where the Hamiltonian H is related to the wave operator \hat{H} in (1). We thus write ρ_Γ in the form

$$\rho_\Gamma(X_s) \approx \sum_{\alpha=1}^{n_e} \sum_{\beta=0}^N \rho_{(\alpha,\beta)} b_\alpha(s) \tilde{P}_\beta(p_s). \quad (7)$$

Here, N is the order of the basis expansion, n_e is the number of elements in the boundary mesh, \tilde{P}_β is a scaled Legendre polynomial of order β and b_α denotes the piecewise constant boundary element basis function. The coefficient vector $\rho_{(\alpha,\beta)}$ in (7) is labelled in terms of the multi-index (α, β) . The matrix approximation B of the ray tracing operator \mathcal{B} is obtained by writing (5) in a weak Galerkin form using the basis approximation (7) and the orthonormal inner product for Legendre polynomials, see [8, 10] for details. Legendre polynomials are chosen since they do not require periodicity for convergence (cf. a Fourier basis) and are relatively simple to implement. For these reasons the method directly extends to an hp - boundary element method as described in [8].

Once the matrix B has been computed, the values of $\rho_{(\alpha,\beta)}$ in (7) are

evaluated using (6) by solving

$$(I - B)\rho_{(\alpha,\beta)} = \rho_{(\alpha,\beta)}^0. \quad (8)$$

Here the source coefficients $\rho_{(\alpha,\beta)}^0$ are obtained by projecting ρ_Γ^0 onto the finite dimensional space spanned by the basis functions as described in [8]. An approximation for the density distribution ρ_Γ on the boundary is obtained after substituting $\rho_{(\alpha,\beta)}$ back into (7). This distribution is then mapped back into the interior region and after projecting onto position space we obtain an approximation for the energy density in (4), see [8] for details. Frequency band calculations are obtained by sampling the results over the frequency band considered.

Recall the splitting into sub-domains Ω_j , $j = 1, \dots, N_\Omega$ introduced earlier. Each sub-domain represents one subsystem for each mode of wave propagation. Coupling between subsystems will be treated as losses in one subsystem and source terms in another. Typical subsystem interfaces are surfaces between the mesh elements of a grid, which may give rise to reflection/transmission due to, for example, sudden changes in material parameters, local boundary conditions or curvature effects. Alternatively, a total transmission of wave energy may occur, for example, when the transmission is between two sub-domains within a homogeneous flat region. We describe the full dynamics in terms of subsystem boundary operators \mathcal{B}_{ij} . Flow between Ω_i and Ω_j is possible only if these sub-domains share a common boundary. We introduce a weight function w_{ij} in (5), which contains (in addition to the usual damping term) reflection and transmission coefficients characterising the coupling between subsystems i and j at the interface. When restricting the implementation to planar sub-domains of simple geometric shape such as

for triangulated surfaces, there is a very efficient way of evaluating the operators \mathcal{B}_{ij} in terms of the so-called *discrete flow mapping* (DFM) technique as described in [1].

Note that the reflection/transmission coefficients depend in general on the angle of incidence of the incoming/outgoing wave and thus on the momentum of the incoming/outgoing ray. In the case of total transmission, the angles of incidence of the incoming and outgoing ray coincide and the transmission coefficient is equal to one. DEA thus incorporates coherent, directed wave transmission through interfaces. This is in contrast to SEA, which assumes diffusive wave fields in each subsystem, that is, wave fields consisting of a uniform superposition of waves from all directions. We will discuss the details about the implementation of interface scattering matrices in a DEA approach in Sec. 2.3. Representing the operator \mathcal{B}_{ij} in a basis function expansion spanning all subsystems leads again to a matrix equation, see [7, 10].

2.3. Interface scattering matrices for plate junctions

Reflection/transmission coefficients are obtained by calculating interface scattering matrices. We focus here on interfaces forming junctions between plates of varying thickness, a setting which is relevant for the benchmark problems discussed in Sec. 3. For DEA, we require local wave solutions taking into account the angle dependence of the corresponding wave scattering. To find the transmission/reflection coefficients of a set of plates being coupled at a common interface (such as depicted in Fig. 3), we follow [11, 12]. In particular, we consider the connection between plates as line junctions, that is, the interior properties of the junction are not modelled and the mass and moment of inertia are neglected.

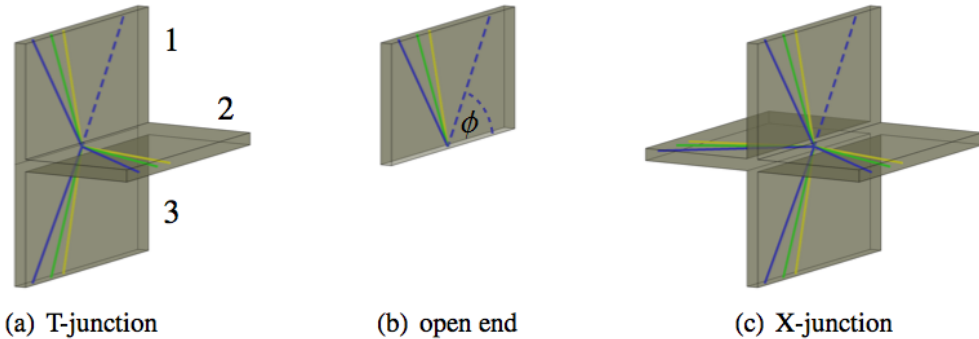


Figure 3: A selection of plate junction configurations depicting an incoming ray at angle ϕ (dashed blue line) and reflected/transmitted rays of the three mode types (solid lines).

Let us consider a line junction which couples n different plates, assuming semi-infinite plates for simplicity. The boundary conditions at the line junction correspond to dynamic conditions involving stresses and moments, and kinematic conditions for the displacement and rotation of all plates. To construct the transmission coefficients we calculate the response of the system with respect to excitation due to an incoming plane wave meeting the interface at an angle ϕ (see fig. 3). The incoming wave has a fixed wavenumber and a characteristic mode, that is, it is of bending (b), pressure (p) or shear (s) type. The outgoing waves typically have components in all plates and are a mixture of all mode types. An evanescent b mode is included to complete the description. Thus, for each plate we have 4 unknown amplitudes for the 4 different wave types. Possible material differences between the plates can lead to different wavenumbers in different plates. For a given forcing with a particular incoming mode in a particular plate, we can solve for the unknown modal coefficients in all plates. In practice, we find the transmission probabilities directly by calculating the ratio of outgoing to incoming normal

power fluxes.

Fig. 4 shows transmission coefficients calculated with the method developed in [11], here for the T-joint in Fig. 3 with material properties described in Sec. 3. In particular, we plot the individual transmission coefficients for a bending mode excitation on the vertical plate in Fig. 3 (a). The coefficients τ_{xy}^{ij} represent the transmission from a wave mode x in plate i to a mode y in plate j with $x, y = b, p, s$ and $i, j = 1, 2, 3$. The plates are numbered as shown in Fig. 3(a), that is, 1 for the vertical plate containing the incident ray, 2 for the horizontal plate and 3 for the other vertical plate. The plot shows the dependence of the coefficients on the (cosine of the) angle ϕ of the incoming ray to the interface. Fig. 4 shows in particular that there is little mode mixing between bending and in-plane modes, and bending modes are predominantly reflected at T-junctions.

In the next section we implement this theory for predicting interface reflection/transmission properties to model wave energy transport in test structures provided by Germanischer Lloyd and Jaguar Land Rover. The results displayed in Fig. 4 are incorporated as part of the weight function w in the finite dimensional approximation of the DEA kernel (5). We assume that the transmission coefficients depend only on the incoming momentum p_s via the angle of incidence ϕ . The outgoing angle is given by Snell's law taking into account refraction due to differences in the wave speed across the interface.

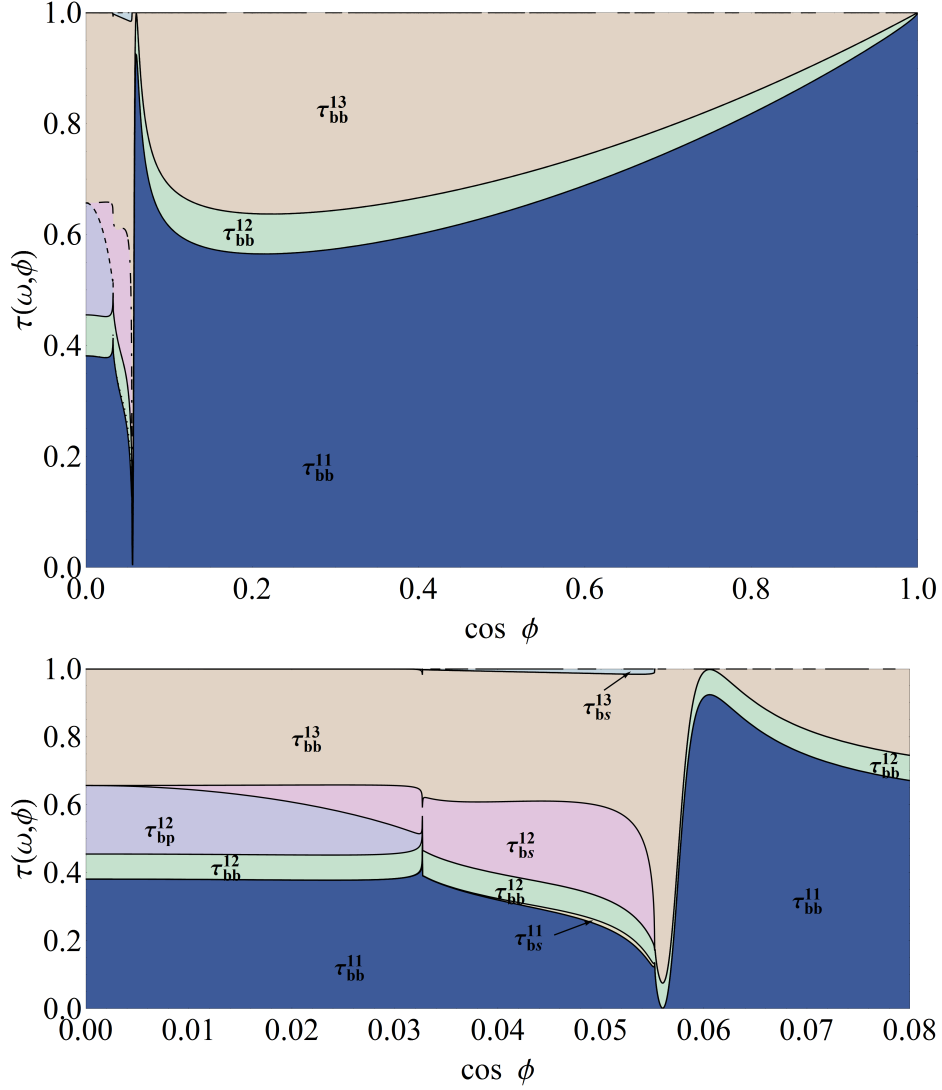
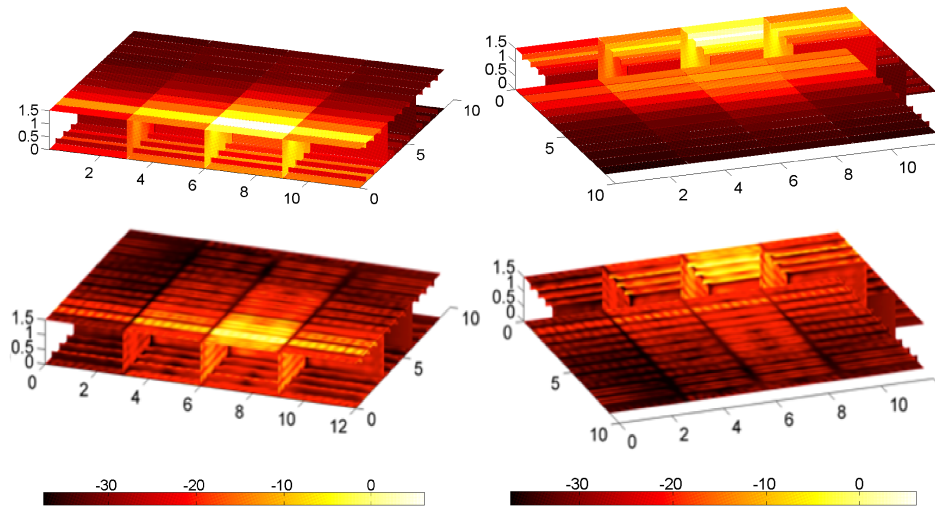
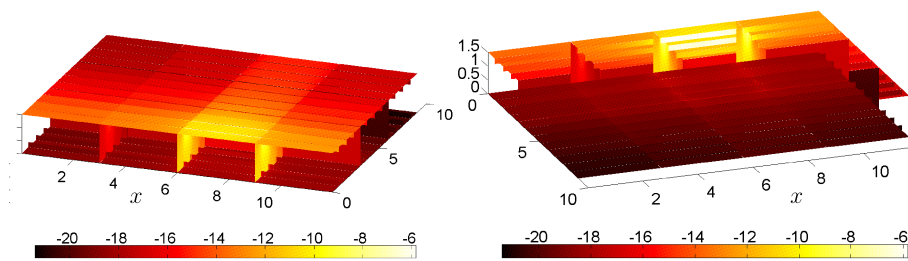


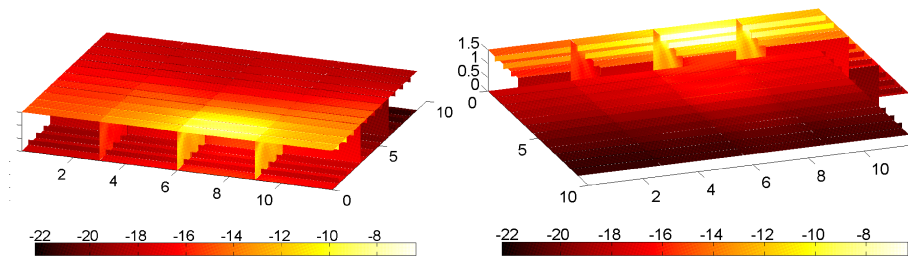
Figure 4: Reflection/transmission coefficients at 200 Hz for a steel T-joint (see fig. 3a) with thickness 8 mm across the two coplanar plates and 16 mm for the perpendicular plate. The normal flux τ_{xy}^{ij} of the outgoing bending ($y = b$), pressure ($y = p$) and shear ($y = s$) modes in each plate $j = 1, 2, 3$ is shown for an incoming bending wave ($x = b$) in plate $i = 1$. ϕ denotes the angle between the incoming ray and the tangent to the plate boundary (see fig. 3). The coefficients τ_{bp}^{11} and τ_{bp}^{13} were too small to be visible in the plot.



(a) Bending mode computed using DEA (upper) and frequency averaged FEM (lower)



(b) Pressure mode computed using DEA



(c) Shear mode computed using DEA

Figure 5: Germanischer Lloyd benchmark example with 40 bending point sources randomly placed within a sub-domain. The plots show the DEA results for the energy density of (a) the bending mode (including verification against FEM), (b) the pressure mode and (c) the shear mode. Energies are displayed on a logarithmic scale, positions are given in meters.

3. Numerical results

3.1. Double-hull structure

We apply the method to a stiffened double bottom test structure provided by Germanischer Lloyd [9] consisting of 8 mm steel plates with 200 mm \times 16 mm stiffeners, see Fig. 5. The distance between the upper and lower plates is 1.5 m and the distance between the side walls is 3 m. The following material parameters for steel are used: Young's modulus $E = 2.1 \cdot 10^{11}$ Pa, Poisson ratio 0.3, and the material density is 7800 kg/m³. We furthermore use hysteretic damping with a damping loss factor 0.03 for all three mode types.

In order to compute the DEA kernel efficiently using DFM techniques, the structure is divided along plate intersections into $N = 212$ rectangular sub-domains as shown in Fig. 5. We further subdivide the boundary of each sub-domain using a boundary mesh with element size 0.2 m or less. In the momentum coordinate we employ an 8th order Legendre basis. The transmission/reflection coefficients are obtained as discussed in Sec. 2.3 and computed directly when evaluating the integrals in (5). Note that due to the regularity of the test structure, we only need to consider the three different types of line joints displayed in Fig. 3. Here the T-joints consist of stiffeners and plates, where the stiffener has twice the thickness of the steel plates. The structure is excited by a set of 40 randomly placed point sources acting on the bending degrees of freedom at 200 Hz in the upper part of the structure, see Fig. 5 (a).

It should be noted that since the in-plane modes have wavelengths of the same order as the size of the plates, the ray approximation (4) is only

valid provided the average is over a wide enough frequency band to include sufficiently many structural modes. The benchmark problem considered here can at 200 Hz also be handled using FEM, see the lower subplots of Fig. 5 (a). For full ship structures, 200 Hz is already in the high frequency regime and beyond the range that can be simulated using FEM due to the sheer size of the structure.

The computation was done on a quad-core processor machine (Intel core i5-2540M cpu 2.60 GHz) with a total computation time of 6.5 minutes. The computation of the matrix coefficients in the $194\,562 \times 194\,562$ sparse matrix with 309 434 904 nonzero entries took 3.5 minutes, solving the linear system with Gauss-Seidel iteration took 2.5 minutes.

Fig. 5 shows the structure and the wave energy density in each of the three modes on a logarithmic scale. The first two rows display (a) the energy stored in the bending mode including the excitation region. The calculations are verified against an FEM result over a frequency band centred on 200 Hz. The agreement is clearly very good, although oscillations on the scale of the wavelength remain in the averaged FEM result that are not captured by our ray model. The energy density in the pressure waves is shown in (b) and the shear energy in (c). As expected, the energy density decreases with the distance to the excitation points due to damping and most energy is contained in the bending mode. However, there are also striking differences in the behaviour shown for the different mode types. The damping in the bending mode is stronger than for the in-plane modes. The transfer from bending energy in the excited plate into pressure wave energy takes place predominantly in the side walls. The energy distribution for the pressure

(p) waves is then surprisingly directional and is dominated by propagation along the side walls in both the x and y directions (as depicted in Fig. 5). In contrast, the bending and shear waves show more uniform behaviour without strong preferential directionality.

3.2. Range Rover shock tower

We now consider the transport of high frequency wave energy in thin shells. High frequency vibro-acoustic models based on an SEA treatment will be unsuitable in these circumstances since complex geometrical features are difficult to include in SEA; obtaining a subdivision of the model into well separated subsystems is thus highly challenging for large moulded castings. DEA can overcome these problems since it can be easily applied in the framework of existing grids for finite element models, requires no choice of subsystem division and incorporates the full geometry and directionality of the energy flow.

We consider the elements of a surface triangulation as our DEA subdomains. Here, the power of the DEA-method together with the DFM implementation becomes obvious as we can immediately work with the meshes provided by the manufacturer, here Jaguar Land Rover, to perform the calculations. Any pre-processing in terms of finding adequate subsystems becomes obsolete. Applying thin shell theory [13], the rays travel along geodesics on the curved surface (provided the radius of curvature is large compared to the wavelength). Ray tracing along geodesics can be implemented on the triangulated surface following [14] by choosing incoming angle equal to outgoing angle at each interface (independent of the angle of intersection of the mesh elements). To incorporate mode mixing and reflection effects in regions of

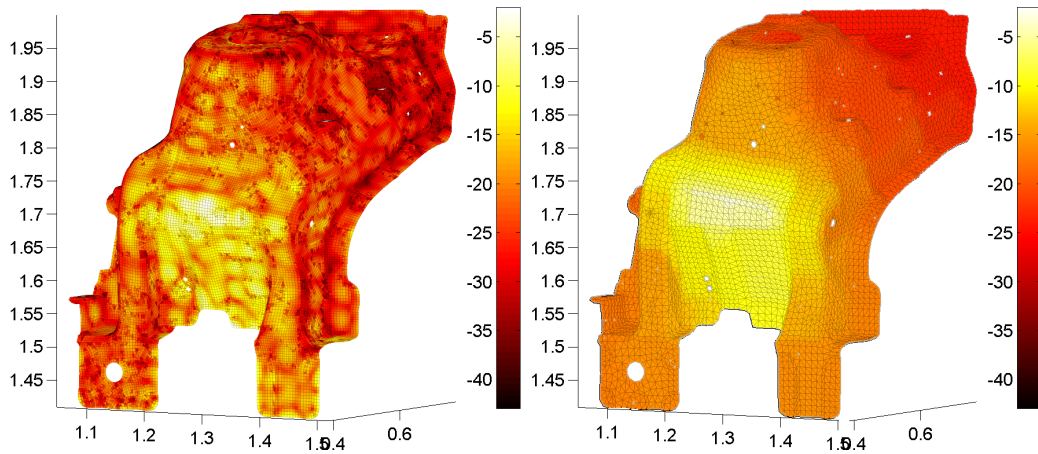


Figure 6: Energy density on a thin aluminium shell (Range Rover shock tower) estimated using an averaged full wave finite element model (left) and a DEA model (right) for 3% hysteretic damping.

strong curvature, we interpret the mesh elements (triangles) as a set of plane plate segments intersecting at the mesh boundaries. The angle of intersection enters into the computation of the scattering matrix giving rise to reflection, transmission and mode conversion as described in Sec. 2.3. Note that the need to deal with non-straight boundaries on the curved surface is avoided by instead working with the triangulation where all boundaries are straight.

The right hand side of Fig. 6 shows the response of a thin moulded aluminium car component (shock tower of a Range Rover) to a point force applied perpendicular to the surface using DEA. The results are compared against a finite element simulation for the full wave model performed using Nastran. In order to maintain a tractable model size for the finite element simulation and to study frequency ranges of industrial interest, the computation is performed at frequencies between 8 kHz and 10 kHz. This approximately corresponds to a third of an octave band centered at 9 kHz. The full

wave kinetic energy is computed in Nastran using shell elements and averaged over 41 evenly spaced frequencies spanning the prescribed range with a typical hysteretic damping level of 3%. The Nastran grid contains 40 670 elements comprising a mix of piecewise linear triangles and quadrilaterals. The DEA computation is performed on a much coarser mesh consisting of 11 623 triangles and a 6th order Legendre polynomial basis in direction space.

As would be expected one sees more oscillation in the full wave model. The prediction of the overall energy flow with DEA is good both in the regions of high and low curvature. In particular, it can be noted in both models that high curvature regions act as barriers for the energy flow. Such geometric features would be entirely absent from SEA-type models and represent a major advance in the simulation of large-scale high frequency vibro-acoustics. The computations in this section were performed with the same quad-core processor machine as in the previous section in 15 minutes.

4. Conclusions

We have presented an approach for modelling the transport of wave energy through complex structures. The proposed method, DEA, interpolates between SEA and ray tracing, taking account of the ray dynamics within the structure and including reflection/transmission and mode conversion at interfaces. Coupling coefficients for more complicated subsystem junctions, such as junctions connecting several plates, have been calculated using a scattering approach and then incorporated into the DEA framework. We have shown that DEA can be implemented on existing mesh grids using the DFM technique.

In particular, DEA was applied to a model vibrational energy distributions in a ship structure provided by Germanischer Lloyd and in a Range Rover body part. Results for a system with several thousand sub-domains and including all three wave modes in plates have been obtained in a competitive computing time-scale of a few minutes. Large scale effects due to non-diffusive wave transport were observed throughout. Our numerical results demonstrate the advantages of a DEA treatment compared to SEA. Damping, directionality and curvature effects can all be modelled providing a detailed analysis in each wave mode with high resolution across the entire structure.

Acknowledgement

The authors wish to thank Christian Cabos and Mark Wilken from Germanischer Lloyd, and Stephen Fisher from Jaguar Land Rover for providing the benchmark problems and for helpful discussions. Support from the EU (FP7 IAPP grant MIDEA) is also gratefully acknowledged.

- [1] D.J. Chappell, G. Tanner, D. Löchel and N. Søndergaard, *Discrete flow mapping: Transport of ray densities on triangulated surfaces*, Proc. R. Soc. A, **469**, 20130153, 2013.
- [2] R. H. Lyon and R. G. DeJong, *Theory and Application of statistical energy analysis* (2nd edn.). Butterworth-Heinemann, Boston MA, 1995.
- [3] R.S. Langley, *A wave intensity technique for the analysis of high frequency vibrations*, J. Sound. Vib. **159**, 483–502, 1992.

- [4] A. Le Bot and A. Bocquillet, *Comparison of an integral equation on energy and the ray-tracing technique for room acoustics*, J. Acoust. Soc. Am. **108**, 1732-1740, 2000.
- [5] A. Le Bot, *Energy transfer for high frequencies in built-up structures*, J. Sound. Vib. **250**, 247–275, 2002.
- [6] G. Tanner, *Dynamical energy analysis – Determining wave energy distributions in vibro-acoustical structures in the high-frequency regime*, J. Sound Vib. **320**, 1023-1038, 2009.
- [7] D. J. Chappell, S. Giani and G. Tanner, *Dynamical energy analysis for built-up acoustic systems at high frequencies*, J. Acoust. Soc. Am., **130**, 1420-1429, 2011.
- [8] D. J. Chappell and G. Tanner, *Solving the stationary Liouville Equation via a Boundary Element Method*, J. Comp. Phys. **234**, 487-498, 2013.
- [9] C. Cabos, H. G. Matthies, *The Energy Finite Element Method Noise FEM*. in Proc. IUTAM Symp. Vib. Analysis of Structures with Uncertainties, St Petersburg, 2009, Eds.: A. K. Belyaev and R. S. Langley, IUTAM series **27** (Springer, Heidelberg, 2011).
- [10] D.J. Chappell, S. Giani and G. Tanner, *Boundary element dynamical energy analysis: a versatile method for solving two or three dimensional wave problems in the high frequency limit*, J. Comp. Phys. **231**, 6181-6191, 2012.
- [11] R. S. Langley and K.H. Heron, *Elastic wave transmission through plate/beam junctions*, J. Sound Vib. **143**, 241-253, 1990.

- [12] R. J.M. Craik, I. Bosmans, C. Cabos, K. H. Heron, E. Sarradj, J. A. Steel and G. Vermeir, *Structural transmission at line junctions: a benchmarking exercise*, J. Sound Vib. **272**, 1086, 2004.
- [13] A. N. Norris and D. A. Rebinsky, *Membrane and Flexural Waves on Thin Shells*, ASME J. Vib. Acoust. **116**, 457-467, 1994.
- [14] R. Kimmel and J. A. Sethian, *Computing geodesic paths on manifolds*, Proceedings of the National Academy of Sciences of the USA **95**, 8431-8435, 1998.